SESD-92-16

HSP-013

SPACE TELESCOPE SCIENCE INSTITUTE

23 April 1992

To : **Systems Engineering Board**

From : Pierre Bély, Olivia Lupie, and Ed Hatter

Subject : **Contribution to the investigation of HSP Proposal 1389 anomalies**

1. Description of the anomaly

Proposal HSP 1389, the *Short-Term Photometric Stability Test*, was designed to determine how immune the HSP observational data is to small amplitude periodicities and noise contributed by the HST or HSP mechanical and electrical systems. The proposal consisted of a 5.6 hour continuous data collection using the UV1 (IDT2) detector in SCP mode with the 1.0" aperture and F240W filter. The target was a known oscillating A5 star of magnitude 9 located in the continuous viewing zone.

The test was executed on day 91.234. The integration time was 0.082399 second per HSP readout. Guiding was with the FGS in coarse track mode, FGS 2 being dominant, and FGS 3 used for roll control.

Figure 1 shows the HSP raw counts obtained during the test, and Figure 2 shows the same data binned over 20 seconds.

Two anomalous features are apparent:

- the counts exhibit an overall 1.2% upward trend as a function of time,
- the counts have a periodic variation with a period equal to that of HST orbit (96 minutes) and a peak-to-peak amplitude of 2.2% of the total counts.

In addition there are several instances of strong count losses which can be directly associated with terminator passages and are due to large telescope line of sight excursions. We will refer to the three most noticeable dropouts as events A, B, and C

2. Calibration of the anomalies

If the effect is pointing-induced, one can estimate the scale of of the anomalies by using the HSP (measured) Point Spread Function. An average PSF in the 1 arcsec aperture (for UV wavelengths but not for the exact filter/aperture/detector combination) was supplied by the HSP team and confirmed to within a few percent by the spatial scan data from the jitter test. This function is shown in Figure 3 , supplied by the HSP team, which gives the

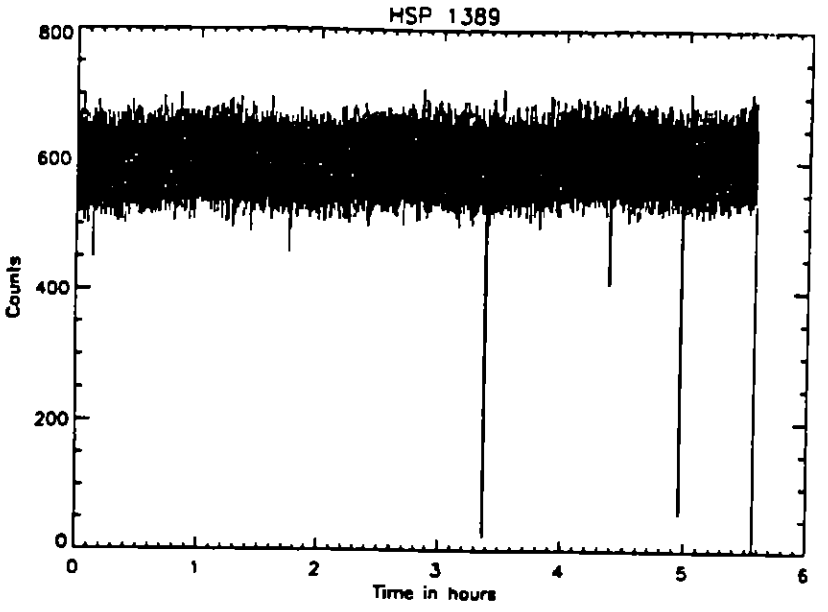

Figure 1

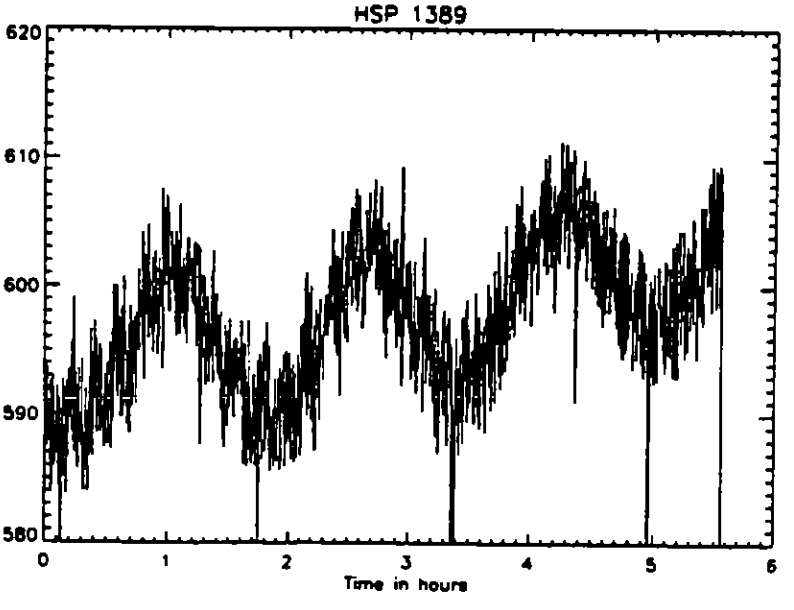

Figure 2

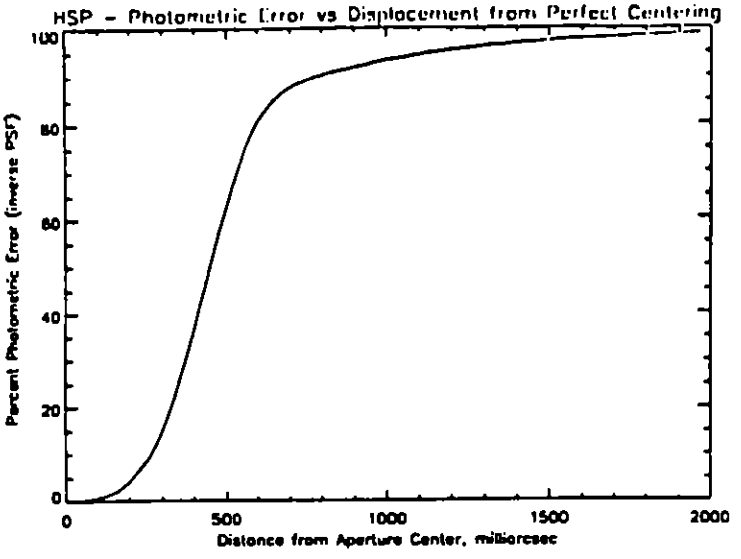
HSP – Photometric Error vs Displacement from Perfect Centering
Percent Photometric Error (inverse PSF)
0
20
40
60
80
100
0
500
1000
1500
2000
Distance from Aperture Center, milliarcsec

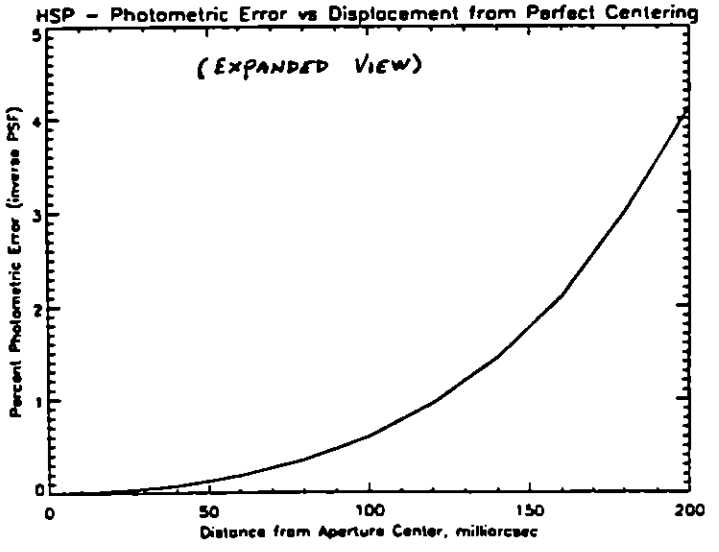
HSP – Photometric Error vs Displacement from Perfect Centering
(EXPANDED VIEW)
Percent Photometric Error (inverse PSF)
0
1
2
3
4
5
0
50
100
150
200
Distance from Aperture Center, milliarcsec

Figure 3

reduction in flux as a function of the position of a star from the aperture center. An additional piece of information is required to perform the calibration however, and that is the position of the star in the aperture.

An initial estimate can be made by verifying the count rates of the star. The initial target acquisition map for this test was taken in an aperture with a different filter. The HSP count rate simulator was used to estimate the change in counts between the filters, assuming the star was well-centered in each aperture (and that the read beams were also aligned). This method is of course limited by the uncertainty in the flux distribution of the star. The HSP PSF, together with the estimated counts of a well-centered star, indicate that the star flux could be no more than ± 25 % different than the one measured. This indicates that the star would then be at the most 0.35 arcsec away from center. Assuming this worst case alignment, a change of 1.1% in the counts (semi-amplitude of the periodic variation) corresponds to ±4 milliarcsec excursion.

We have also attempted to estimate the amplitude of the anomaly by comparing the signature of the large terminator-induced oscillations seen in both the HSP data and the FGS. Unfortunately, this leads to very inconsistent results because of the poor sampling rate of the FGS data (1 second) and the generally poor response of the FGSs in coarse track.

Another method is to analyze the detailed structure of those large terminator induced oscillations seen in the HSP science data set alone. In particular, Event C, shown in Figure 4 oscillates at 0.6 Hz, a prevalent frequency whose origin is the solar array in-plane motion. The 3 components of event C can be 'unfolded' to show an action consistent with a large excursion in one direction, followed by an opposite motion (middle component), and a swing back to a final excursion in the original direction before settling out. The fact that the middle component does not extend as far as the other two suggests that the star is not centered, even if linear damping of the motion is assumed. We can then reconstruct the position of the star in the aperture using the relative depths of the components, the assumption of linear damping, and the PSF curve. The results are that the amplitude of the first component is 0.65 arcsec and the star is 0.1 arcsecond away from the aperture center. Given this geometry, the periodic oscillations have an excursion amplitude of ±30 milliarcsec .

Although there is a dispersion in the amplitudes obtained by the different methods, the data and analysis suggest that the excursion amplitude would be on the order of tens of milliarcsec rather than hundreds of milliarcsec.

3. Pointing as an explanation

The most obvious possibility for explaining the sinusoidal and trend effects is that they are the result of the motion of the star in the aperture. Since the observation was guided with the FGS, the effect could be the result of a pointing change in the dominant FGS (for example by thermal effects). The dominant FGS would then erroneously be driving the entire HST, resulting in a motion of the HSP line of sight, but with no signature in the FGS data (the

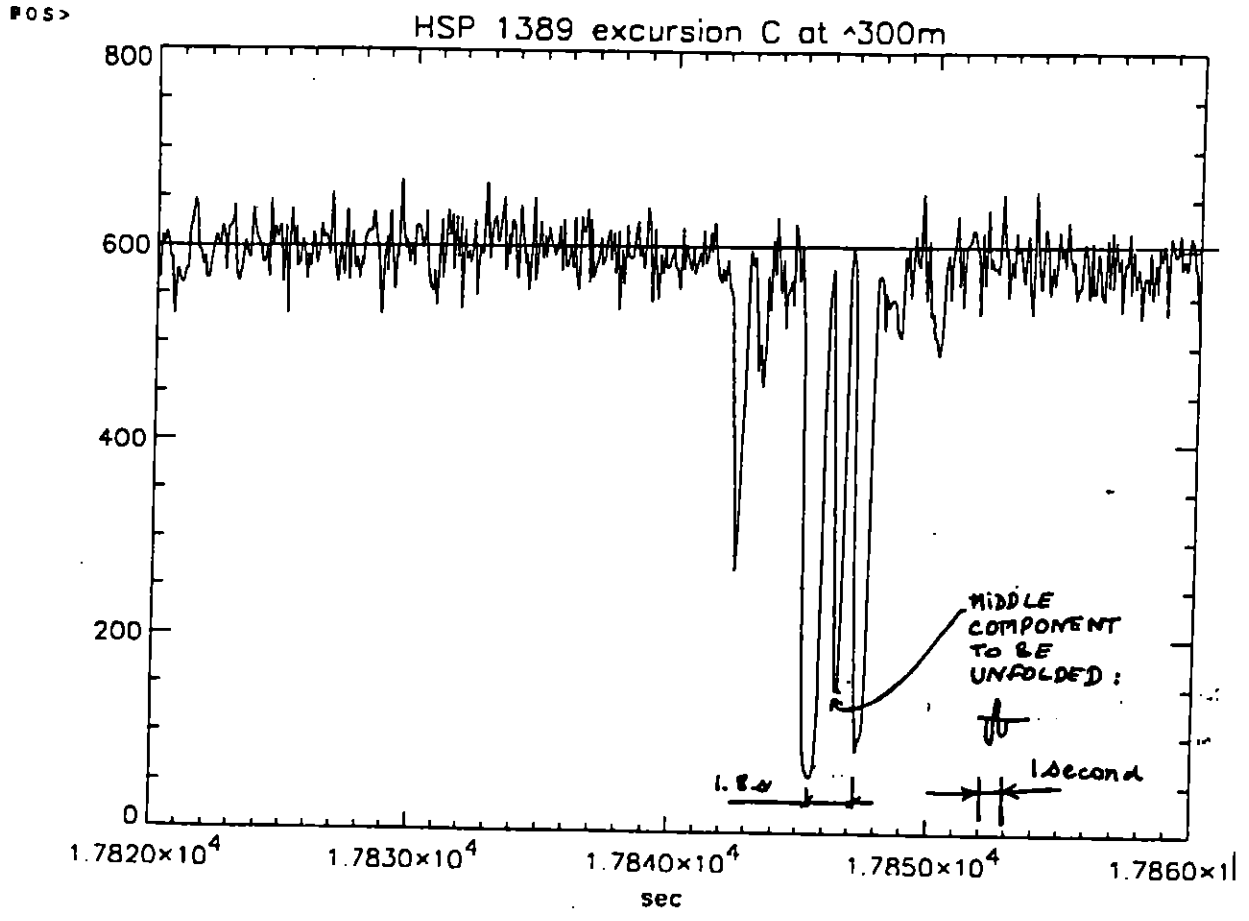
POS>
HSP 1389 excursion C at ^300m
800
600
400
200
0
1.7820×10^4
1.7830×10^4
1.7840×10^4
1.7850×10^4
1.7860×1
sec
MIDDLE COMPONENT TO BE UNFOLDED :
1.8 s
1 Second

Figure 4

Pointing Control System compensating for any potential drift in the dominant FGS). An alternate possibility would be an incorrect calculation of the velocity aberration.

To test this "pointing error" hypothesis, we have reconstructed the absolute pointing on the sky of each of the two FGSs and of the HSP aperture as a function of time, based on the FGS telemetry data, and after removing the effect of the velocity aberration. The method used is as follows:

First the position of the two guide stars is determined every second from the telemetry monitors giving the center of nutation of the two FGSs.

Then, the effect of differential velocity aberration between the two FGSs and the HSP is removed. The differential velocity abberation is calculated from the definitive HST orbital ephemeris for the velocity aberration component due to HST orbital velocity, and from the sun ephemeris for that due to the earth velocity. Because the target is close to the orbital pole, the amplitude of the velocity aberration due to the HST orbital velocity is quite large, on the order of ±5 arcseconds, but the differential aberration in the field of view is very small (±2 mas between the two guide stars). The effect of the earth velocity is again very large in absolute value (20 arcseconds), but the differential effect in the field of view is small (0.5 mas) and its change over the 5.6 hours of the test is essentially negligible (about 0.03 mas).

Then, the attitude of the spacecraft is derived from the instantaneous unaberrated position of the two guide stars. Since the position of the two guide stars supply 4 values, while only 3 are needed to determine the spacecraft attitude, the data is solved for a least square fit approximation where equal weight is given to the two guide star positional information (see Appendix A).

Finally, the instantaneous HSP line of sight is obtained by applying, to the attitude data, the transformation matrix corresponding to the location of the HSP aperture in question.

The reconstructed pointing data has been smoothed over 150 seconds to reduce the effect of jitter which is on the order of 20 milliarcsecond rms.

The results are presented in Figure 5 which shows the reconstructed pointing of HSP as a function of time, and in Figure 6 which shows the variation of the separation between the two guide stars in FGS 2 and 3. For reference, Figure 7 gives the respective location of the two guide stars and the HSP aperture in the focal plane.

The HSP reconstructed pointing appears extremely constant (to a few milliarcseconds, with the effect of jitter removed by smoothing), and certainly does not show any variation of the amplitude required to explain the anomaly.

It is not possible to derive the absolute stability of the guiding FGSs from this data. However, the separation between the two guide stars is fairly constant, suggesting that the two FGS are indeed stable at the level of a few milliarseconds. If the FGSs were indeed moving but their separation remained constant, the line of sight motion of the roll FGS (FGS 3) would have to be roughly the same amplitude as that of the dominant FGS and in the perpendicular direction with respect to its own body. Assuming that such effects are thermally driven, this is a very unlikely situation in view of the orientation of the two FGS with respect to sun.

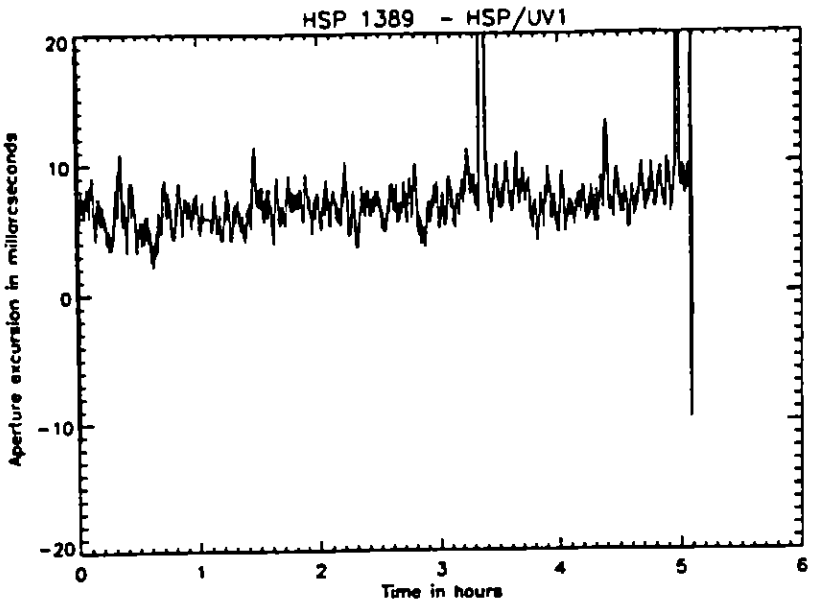

Figure 5

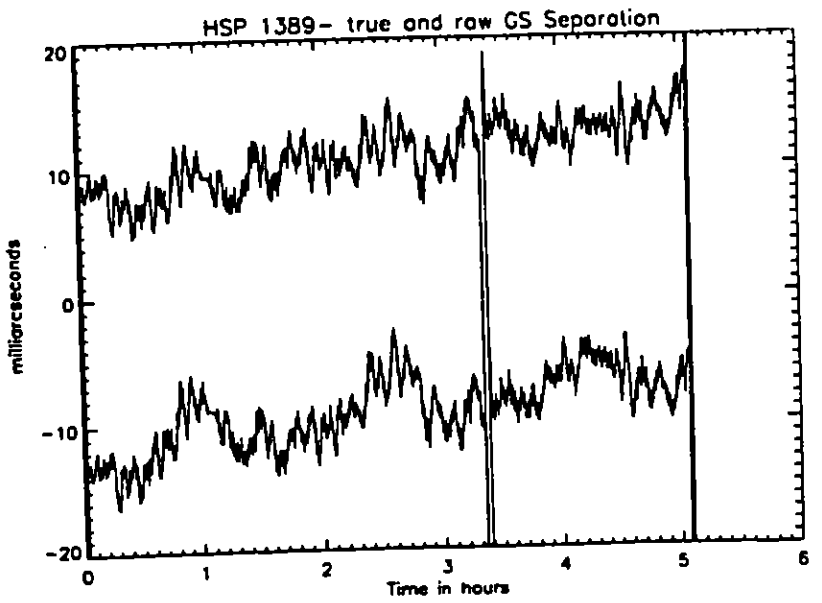

Figure 6

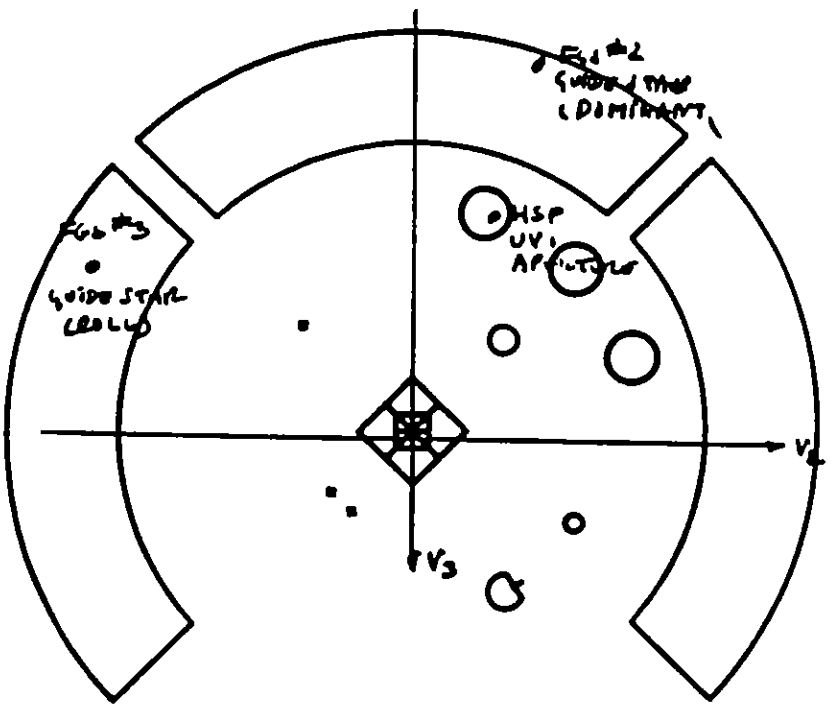

Figure 7

Although

~~If~~ the separation between the two guide stars does not show any orbital change, it does exhibit a slight increase with time, on the order of 7 mas. This is likely attributable to the change of pointing in the two FGSs during their thermal stabilization following the change of attitude.

It must be noted that because of the least square fit method employed, in which equal weights are given to the two guide stars, the reconstructed HSP line of sight does not show the drift seen in the guide star separation (the solution assumes that the two guide stars are moving away from each other in equal amount from their initial position).

However, even if one was to assume that all of the effect is due to FGS 2 motion, and taking the geometry of the two guide stars and the HSP aperture into account, the induced displacement of the HSP aperture would not be more than about 8 mas, not enough to explain the observed drift part of the effect, and would still leave the periodic part of the effect unexplained.

We conclude from this analysis that, telescope pointing is not likely the main cause of the anomaly: the FGS do appear very stable, and the velocity aberration correction seems to be applied correctly.

4. Straylight as an explanation

Another possibility is that the HSP observation was affected by straylight during the passage over bright earth. Indeed, because the target is in the continuous viewing zone, the line of sight approaches closely to the earth limb.

The angle between the line of sight and the earth limb is shown on Figure 8, together with the HSP flux counts (smoothed and on an arbitrary scale).

There are two reasons why straylight cannot be an explanation of the anomaly.

First and foremost, the closest approach to the bright earth limb is about 20 degrees. From our straylight model (confirmed by the Observatory Level Test "Baffle"), at this angle the flux added by the bright-earth induced straylight is on the order of 18th magnitude per arcsecond square. Since the HSP aperture is 1 arcsecond in diameter, and the star is of magnitude 9, this would represent an additional count rate of about 2×10^{-4} which is 100 times less than what is observed.

The second reason is that the time profile of the straylight flux is not consistent with the HSP counts variation. If due to straylight, the HSP counts should flatten out during the dark earth passage, and peak when the limb angle reaches the minimum value, features which are not seen in the data.

5. Magnetic field as an explanation

Another possibility is that variations in the magnetic field would somehow deflect the readbeam resulting in a mismatch between the readbeam and the aperture.

Figure 9 is a plot of the magnitude of the magnetic field perpendicular to the HST V1 axis with respect to time. The signature of the earth's magnetic

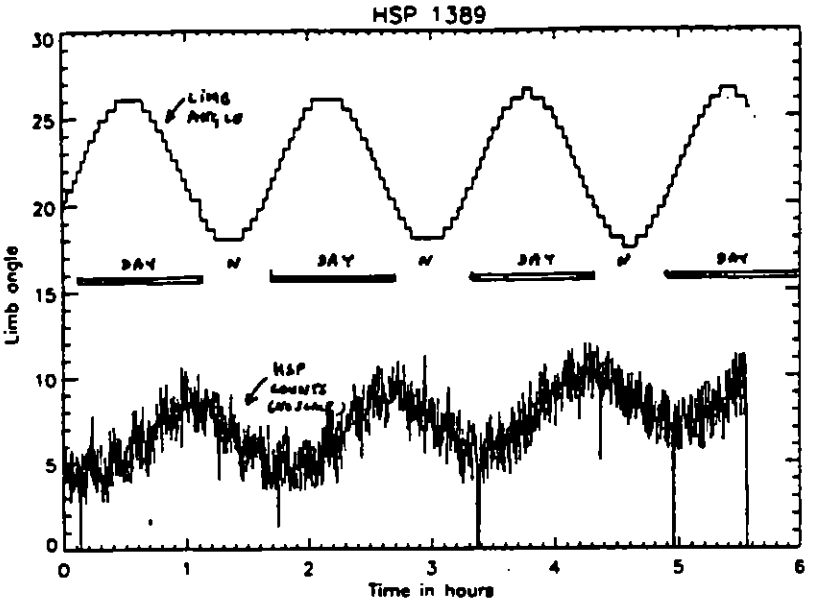

Figure 8

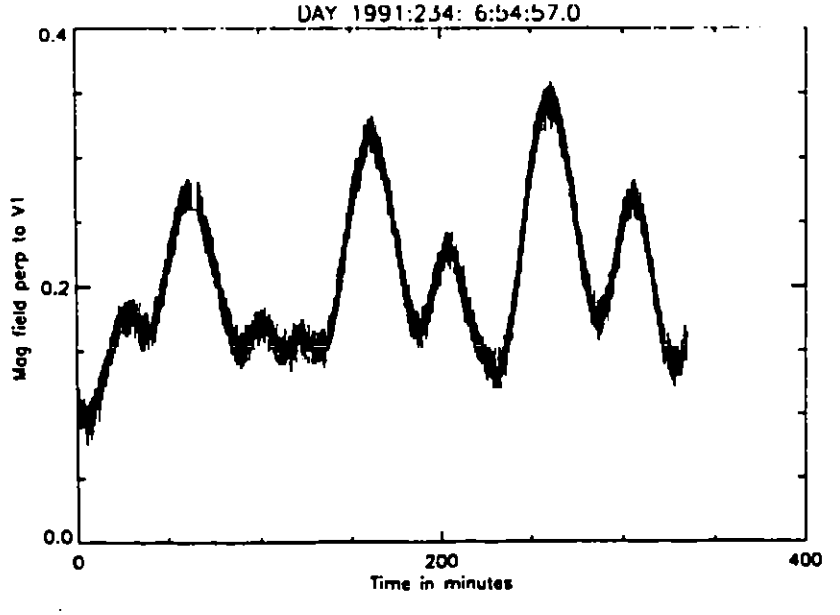

Figure 9

field clearly does not correlate with the sinusoidal orbital variation in the HSP data, and it is therefore unlikely that the earth magnetic field would be responsible for the anomaly.

6. Thermal variations as an explanation

Thermal analysis of the HSP has shown that with the exception of the ODS P3 radiator temperature, there does not appear to be a significant variation in internal temperatures during the 5.6 hours of the observation. A brief description of our findings follows:

As shown on Figure 10, the temperature of the detector electronics, system controller, RIU, and PCDS temperatures all prove to be nominal for the data collection period. In all cases the signature is a steady rise with no evidence of thermal oscillation.

Figure 11 shows the temperature of other selected areas within the HSP.

The HSP forward and aft bulkhead temperatures also prove to be nominal The bulkheads experience a steady rise in temperature with an increase of approximately 1.5 deg C in forward bulkheads 1 and 2, and 2 deg C in aft bulkhead 1 and 2. In all cases there is no indication from telemetry of thermal variation on an orbital period.

Mount (latch) points A and C experience a steady rise in temperature over the 5.6 hour period. Mount point A temperature increased 1.6 deg C, mount point C increased 2.4 deg C. Mount point B remained steady for most of the 5.6 hour period with an increase of 0.5 deg C near the end of the data collection. In all cases however there is no indication of thermal variation on an orbital period.

The HSP ODS P2 radiator experienced a steady rise in temperature with an increase of approximately 2 deg C and no indication of thermal oscillation over the 5.6 hour period. However, the ODS P3 radiator experienced a 2.75 deg C increase in temperature over 5.6 hour period with a thermal variation of approximately 0.75 deg C per orbit.

The ODS P3 radiator temperature is shown on Figure 12 together with the HSP counts (no scale) to show how similar the two variations are. Both show the same "saw tooth" shape, with a rise longer than the fall, and the same kind of overall upward "trend". However, the radiator temperature lags the count data by approximately 15 minutes.

It is also interesting to note that a plot of the FGS2 radiator temperature possesses the same characteristics seen in the science data and the HSP ODS P3 radiator temperature. The similarity to the latter is not surprising since EGS2 and HSP ODS radiators are located on the same side of the aft shroud and would therefore be subject to similar thermal changes.

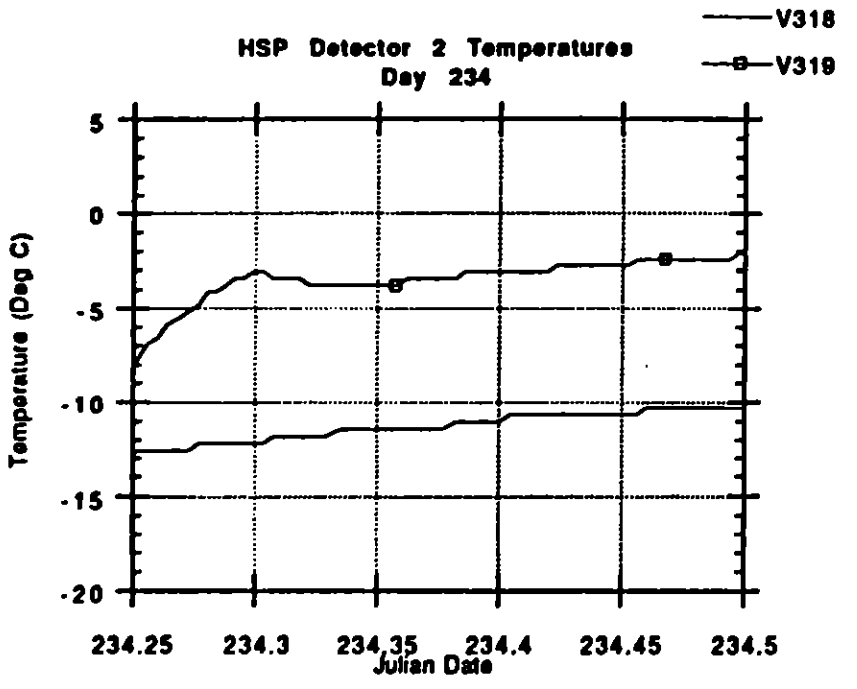
HSP Detector 2 Temperatures
Day 234
V318
V319
Temperature (Deg C)
5
0
-5
-10
-15
-20
234.25
234.3
234.35
234.4
234.45
234.5
Julian Date

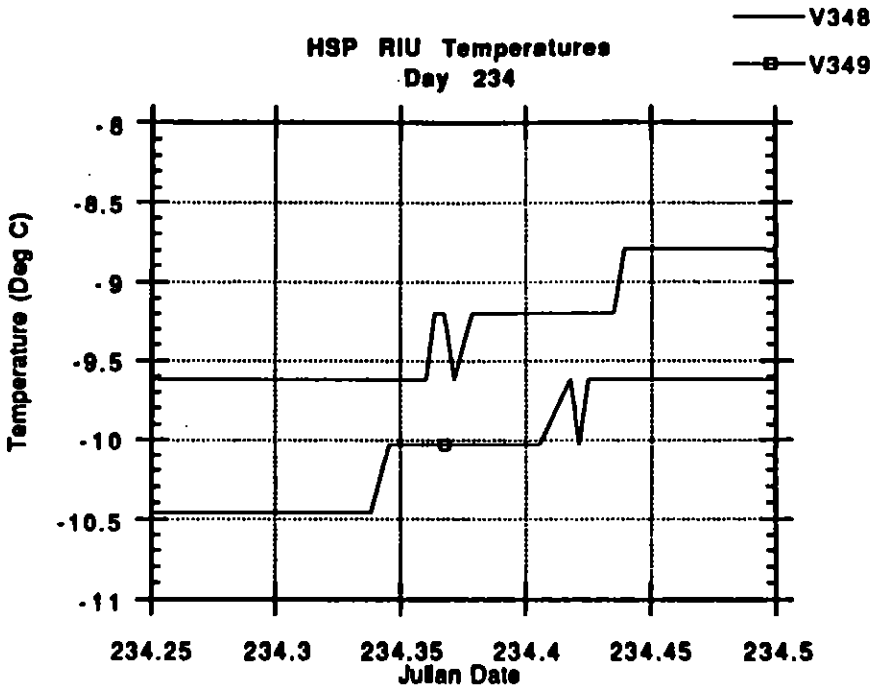
HSP RIU Temperatures
Day 234
V348
V349
Temperature (Deg C)
-8
-8.5
-9
-9.5
-10
-10.5
-11
234.25
234.3
234.35
234.4
234.45
234.5
Julian Date

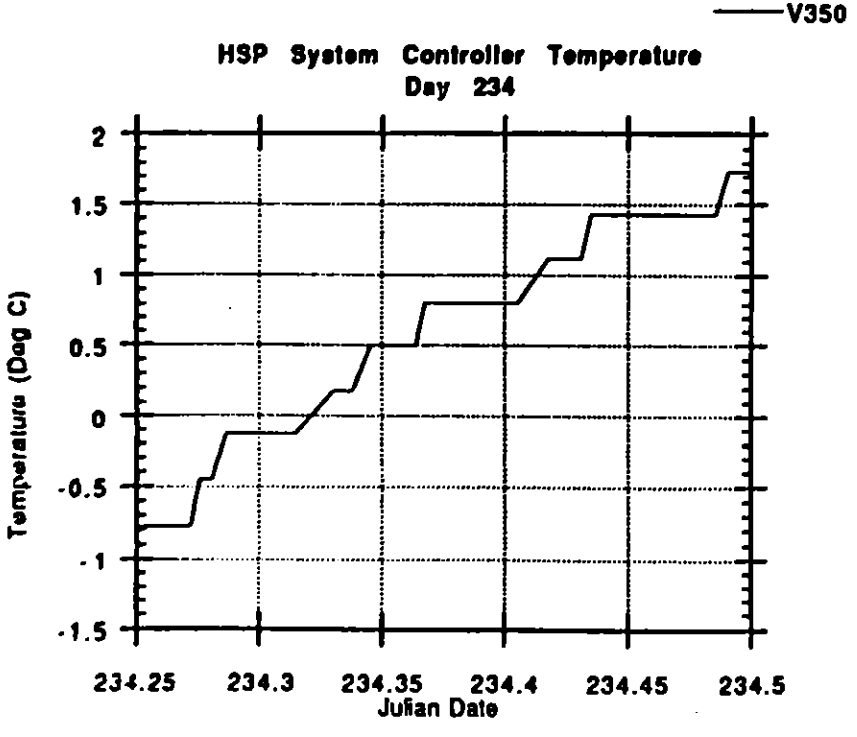
HSP System Controller Temperature
Day 234
V350
Temperature (Deg C)
2
1.5
1
0.5
0
-0.5
-1
-1.5
234.25
234.3
234.35
234.4
234.45
234.5
Julian Date

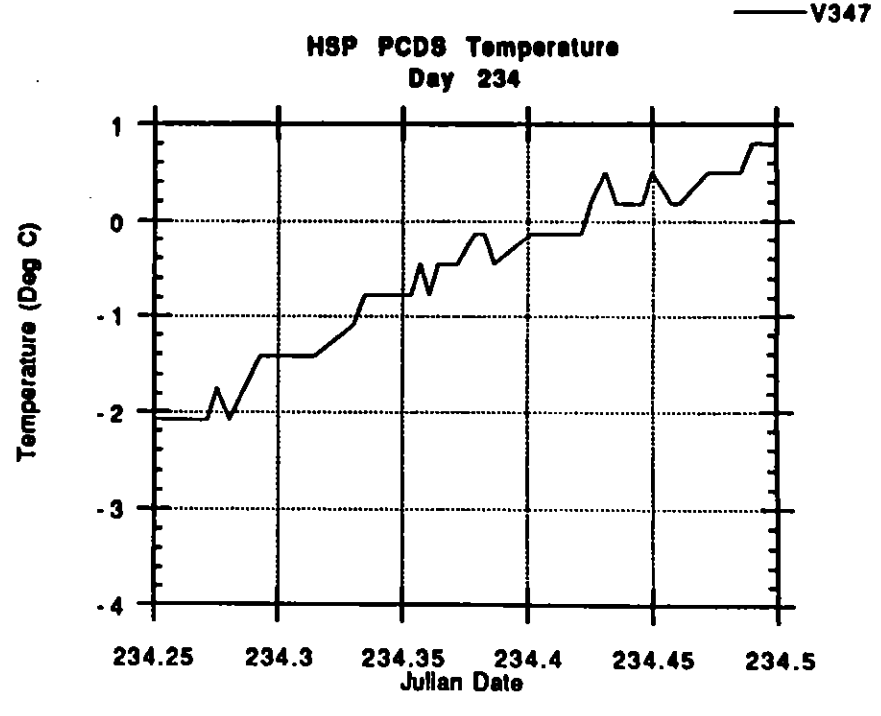
HSP PCDS Temperature
Day 234
V347
Temperature (Deg C)
1
0
-1
-2
-3
-4
234.25
234.3
234.35
234.4
234.45
234.5
Julian Date

Figu 10

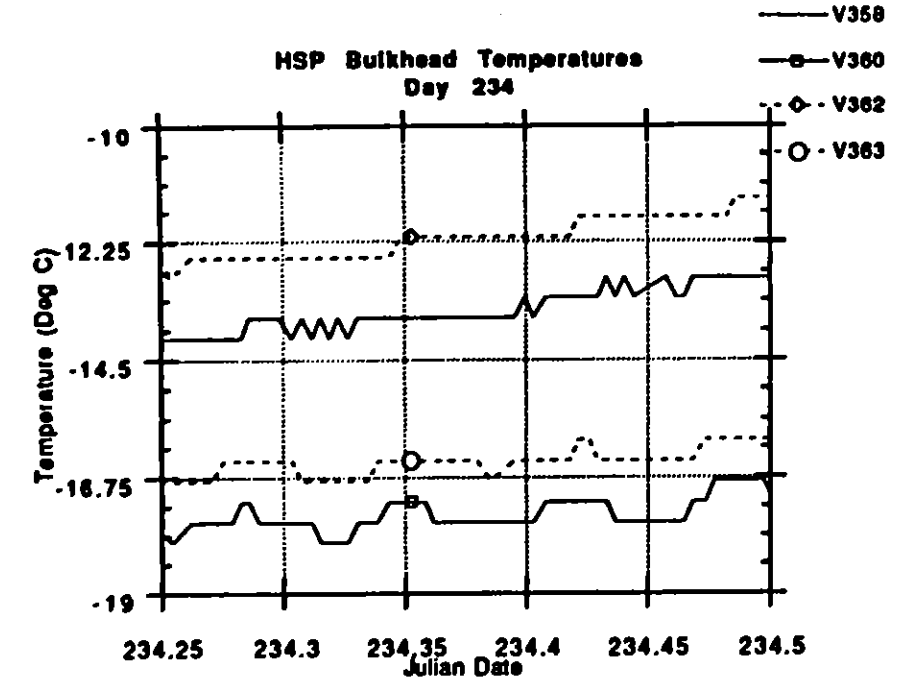
HSP Bulkhead Temperatures
Day 234
V358
V360
V362
V363
Temperature (Deg C)
-10
-12.25
-14.5
-16.75
-19
234.25
234.3
234.35
234.4
234.45
234.5
Julian Date

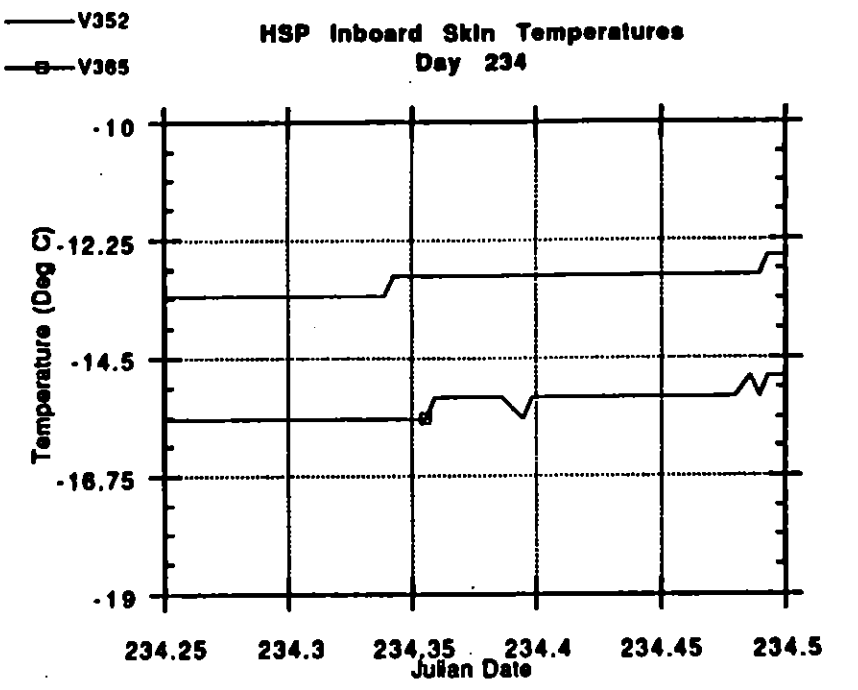
HSP Inboard Skin Temperatures
Day 234
V352
V365
Temperature (Deg C)
-10
-12.25
-14.5
-16.75
-19
234.25
234.3
234.35
234.4
234.45
234.5
Julian Date

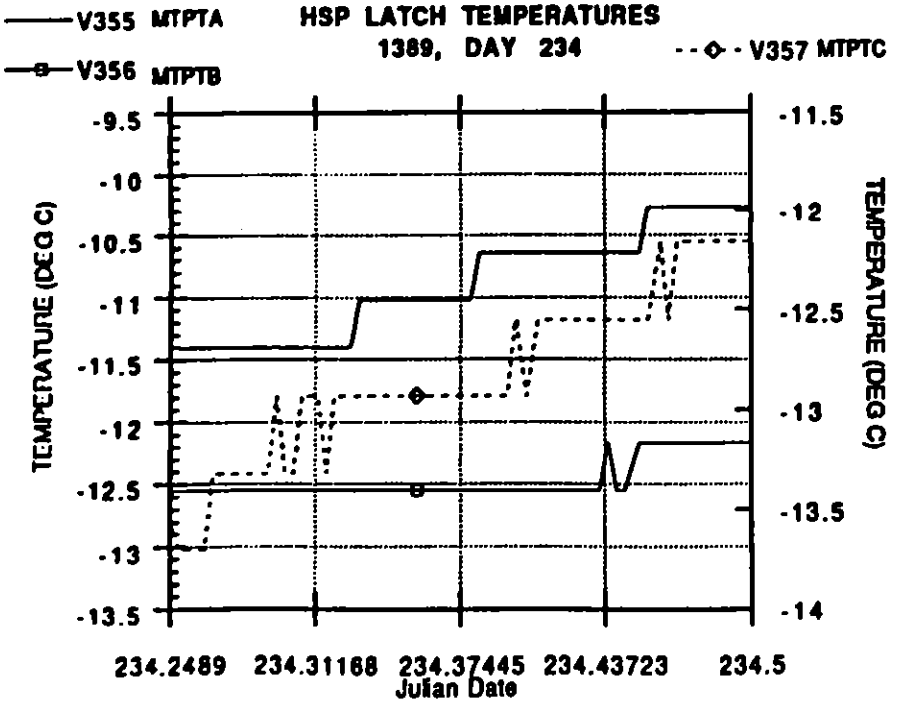
HSP LATCH TEMPERATURES
1389, DAY 234
V355 MTPTA
V356 MTPTB
V357 MTPTC
TEMPERATURE (DEG C)
-9.5
-10
-10.5
-11
-11.5
-12
-12.5
-13
-13.5
-11.5
-12
-12.5
-13
-13.5
-14
234.2489
234.31168
234.37445
234.43723
234.5
Julian Date

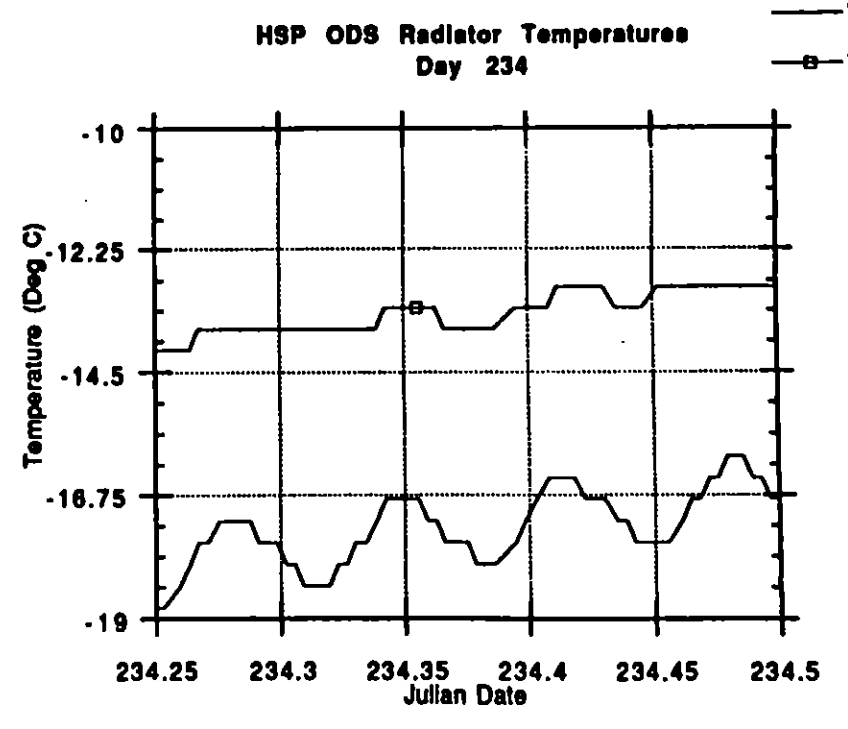
HSP ODS Radiator Temperatures
Day 234
V351
V361
Temperature (Deg C)
-10
-12.25
-14.5
-16.75
-19
234.25
234.3
234.35
234.4
234.45
234.5
Julian Date

Figure 11

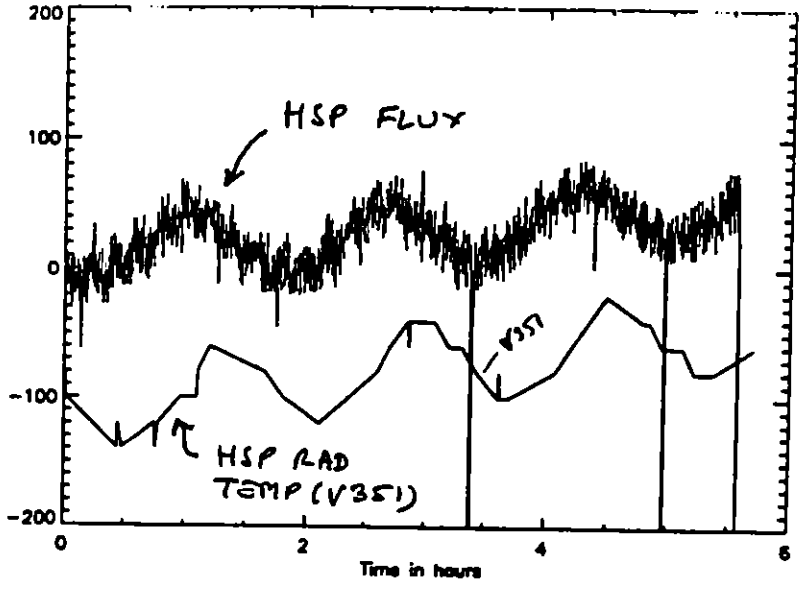
200
100
0
-100
-200
0
2
4
6
Time in hours
HSP FLUX
HSP RAD
TEMP (V351)
V351

Figure 12

7. Electrical effects as an explanation

There is no indication from telemetry of anomalous performance of the HSP electronics which could produce or contribute in anyway to the signal seen in the HSP science data.

The overall spacecraft bus current, shown in Figure 13 does naturally exhibit a periodic behavior resembling that of the HSP counts. The shape however is not quite consistent and there is no known mechanism to explain a possible causal effect.

8. Conclusion

In conclusion, we have no consistent explanation to offer.

Our analysis does not support a pointing, straylight, magnetic, or electrical origin.

The HSP thermal data does exhibit a time profile very similar to the science data, but has a lag which suggests that there is no causal relationship.

9. Acknowlegdments

We want to thank Lisa Walters, Xuyong Liu, J.C. Hsu, John Hershey for their assistance in the data analysis.

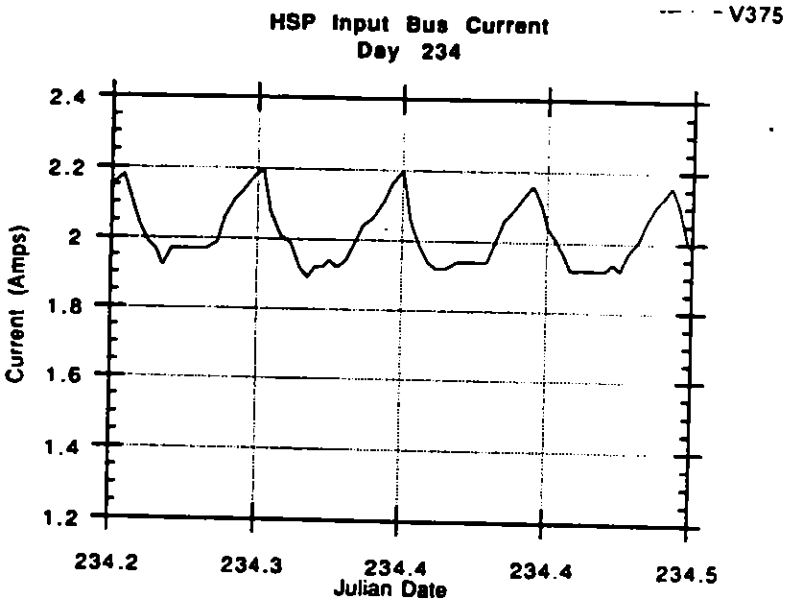
HSP Input Bus Current
Day 234
V375
2.4
2.2
2
1.8
1.6
1.4
1.2
Current (Amps)
234.2
234.3
234.4
234.4
234.5
Julian Date

Figure 13

Ball - Sec VI

LOS RECONSTRUCTION - PLANAR APPROXIMATION -

Guide star coordinates : $t=0$ $\begin{vmatrix} x_1 \\ y_1 \\ x_2 \\ y_2 \end{vmatrix}$ $\begin{matrix} \} \text{FGS 1} \\ \\ \} \text{FGS 2} \end{matrix}$ $t=t$ $\begin{vmatrix} x_1' \\ y_1' \\ x_2' \\ y_2' \end{vmatrix}$

Transformation $\begin{vmatrix} X_0 \\ Y_0 \\ \theta \end{vmatrix}$

System of 4 equations with 3 unknowns :

$$\begin{vmatrix} x_1' = X_0 + x_1\cos\theta - y_1\sin\theta \\ y_1' = Y_0 + x_1\sin\theta + y_1\cos\theta \\ x_2' = X_0 + x_2\cos\theta - y_2\sin\theta \\ y_2' = Y_0 + x_2\sin\theta + y_2\cos\theta \end{vmatrix} \begin{matrix} \} \text{FGS 1} \\ \\ \} \text{FGS 2} \end{matrix}$$

θ is small, hence $\cos\theta = 1$, $\sin\theta \simeq \theta$, system can be rewritten as:

$$A\begin{pmatrix} X_0 \\ Y_0 \\ \theta \end{pmatrix} = \begin{pmatrix} \xi_1 \\ \eta_1 \\ \xi_2 \\ \eta_2 \end{pmatrix} \qquad \text{where : } A = \begin{pmatrix} 1 & 0 & -y_1 \\ 0 & 1 & x_1 \\ 1 & 0 & -y_2 \\ 0 & 1 & x_2 \end{pmatrix}$$

and: $\xi_1 = x_1' - x_1$ $\quad \xi_2 = x_2' - x_2$

$\eta_1 = y_1' - y_1$ $\quad \eta_2 = y_2' - y_2$

Solve for least square approximation :

$$\begin{pmatrix} X_0 \\ Y_0 \\ \theta \end{pmatrix} = (A^T A^{-1}) A^T \begin{pmatrix} \xi_1 \\ \eta_1 \\ \xi_2 \\ \eta_2 \end{pmatrix}$$

$$X_0 = \frac{1}{S}\left[(y_1+y_2)(x_1-x_2)(\eta_2-\eta_1) - (\xi_1+\xi_2)\left[(x_1-x_2)^2 - 2y_1y_2\right] - 2(y_1^2\xi_2 + y_2^2\xi_1)\right]$$

$$Y_0 = \frac{1}{S}\left[(x_1+x_2)(y_1-y_2)(\xi_2-\xi_1) - (\eta_1+\eta_2)\left[(y_1-y_2)^2 - 2x_1x_2\right] - 2(x_2^2\eta_1 + x_1^2\eta_2)\right]$$

$$\theta = \frac{2}{S}\left[(y_1-y_2)(\xi_1-\xi_2) + (x_1-x_2)(\eta_2-\eta_1)\right]$$

where $S = -2\left[(x_1-x_2)^2 + (y_1-y_2)^2\right]$